Epitaxial HoN thin films: An investigation of the structural, electronic, and magnetic properties

V. M. Pereira [1] A. Meléndez-Sans [1] C. F. Chang [1] C.-Y. Kuo [1,2,3] C. T. Chen [2]
L. H. Tjeng [1] and S. G. Altendorf [1]

[1]*Max Planck Institute for Chemical Physics of Solids, Nöthnitzer Str. 40, 01187 Dresden, Germany*
[2]*National Synchrotron Radiation Research Center, 101 Hsin-Ann Road, 30076 Hsinchu, Taiwan*
[3]*Department of Electrophysics, National Yang Ming Chiao Tung University, Hsinchu 30010, Taiwan*

We report our study on the growth of HoN thin films on MgO (100) and LaAlO$_3$ (100) substrates. By using molecular beam epitaxy, we thermally evaporate holmium in an atmosphere of molecular nitrogen, forming HoN at slow rates, moderate temperatures and pressures. We are able to carefully and systematically vary the growth conditions, thereby tuning the nitrogen content of our samples. We explore the differences in the growth window by looking at the crystalline structure and composition of the films deposited on the different substrates. We find that HoN has an epitaxial, well-ordered growth on LaAlO$_3$, in contrast to the three-dimensional growth that occurs on MgO. Using a combination of *in situ* electron diffraction and x-ray spectroscopies, as well as *ex situ* x-ray diffraction and SQUID magnetometry, we investigate the structural, electronic, and magnetic properties of the epitaxial HoN films.

I. INTRODUCTION

The attractive combination of electronic and magnetic properties of the rare-earth nitrides (RENs) has generated a lot of interest in these materials since the early 1960s. However, recurring problems with the lack of stoichiometry of the samples and quick oxidation when in contact with air have created contradicting results and considerable debate, causing a dimming of the research until the turn of the century. In the last decade there has been a resurgence of attention to this series, accompanied by the increasingly popular field of spintronics, where these materials may have many potential applications [1–4].

The new studies on the rare-earth nitrides have, in their majority, focused on the investigation of thin films grown under vacuum conditions, which allows an improved control of the cleanliness of the environment and of the composition of the samples. However, despite the advances of thin film technologies, the study of REN films presents significant challenges up to today, due in part to the lack of suitable substrates. These materials crystallize in a cubic rocksalt structure, with lattice parameters varying between 5.31 Å and 4.76 Å across the series [5]. For HoN it is 4.87 Å. Substrates with the same crystal structure, with a small lattice mismatch, and that do not react with the rare earth are very limited. This limitation strongly impacts the realization of well ordered films. In fact, many studies have reported the growth on highly mismatched substrates, resulting in polycrystalline samples [6–13]. (100)-

oriented REN epitaxial films have been successfully grown on MgO (100) [14], YSZ (100) [15–18], and Si (100) [19], although the films are still generally rough due to defects or the formation of a parasitic interface layer. Moreover, conflicting results are still being published and fundamental questions remain unanswered. The quality of the samples, poor control of the stoichiometry, and potential degradation may contribute to this uncertainty. Given the recognized importance of a precise control of the composition in this class of materials, it is surprising that there are comparatively few detailed reports on the growth of REN films [14,15,19–21].

Additionally, most thin film studies report high growth rates, temperatures, and nitrogen pressures using various deposition methods like pulsed laser deposition [15,16,18,22], rf magnetron sputtering [23,24], ion-assisted deposition [8,9], and molecular beam epitaxy [13,19,20,22], which may contribute to the formation of defects in the samples. In this paper, we aim for the growth of a REN by molecular beam epitaxy (MBE) in true ultrahigh vacuum (UHV) base pressures, at slow rates, low temperatures, and moderate nitrogen pressures, using the example of HoN. In contrast to GdN [4,13–16,20,25–28] and SmN [2,7,12,19,28–32], this material has not gathered as much attention in the recent years [8,9], and a thorough investigation of the growth and stoichiometry is still lacking. Holmium evaporates at moderately high temperatures ($<1000\,^\circ$C), enabling the use of standard effusions cells and thus avoiding heavily out-gassing, high-temperature e-beam evaporators, which are usually used, e.g. for gadolinium [13,26]. In addition, holmium has only one stable valence state of 3+, in contrast to samarium and europium, and reacts with molecular nitrogen to form HoN, bypassing the need for activated nitrogen sources such as ion or plasma sources or reactive nitrogen precursors as ammonia that represent an additional source of contamination in the growth process. Using these careful preparations and clean growth conditions,

we approach a maximal control over the stoichiometry and quality of the sample, which is essential for the identification and understanding of the truly intrinsic properties of the material.

Similarly to other RENs, modern calculations predict HoN to be a semiconductor [33,34], and an optical gap of 1.48 eV has been experimentally observed for thin films [8]. Furthermore, the full magnetic moment associated with the Ho^{3+} ion is quite large, with $gJ = 10 \mu_B$. However, different experiments on bulk samples [35–39] and thin films [9] have consistently reported smaller values than theoretically expected for a simple ferromagnet. Early neutron diffraction experiments have proposed a complex magnetic structure for this material [35], with different authors describing its behavior as ferromagnetic [36,38], ferrimagnetic [35,37], and metamagnetic [39]. Nonetheless, the different studies seem to conclude that there is a spontaneous magnetization in HoN with a Curie temperature between 13 and 18 K.

In this paper we report a comprehensive growth study of HoN synthesized by molecular beam epitaxy (MBE) in UHV. Our choice of substrates enables the growth of epitaxial HoN films, in contrast to the few existing reports of polycrystalline samples [8,9]. A comparison of the growth on two different substrates further allows to investigate the influence of the lattice mismatch on the films. The quality of the epitaxial films is characterized by means of electron and x-ray diffraction, x-ray spectroscopies, and magnetometry.

II. EXPERIMENT

HoN thin films were grown by MBE on epi-polished MgO (100) and LaAlO$_3$ (LAO) (100) substrates purchased from Crystec GmbH and Crystal GmbH, respectively. Prior to the deposition, the substrates were annealed *in situ* at 500–600 °C for 2 hours in an oxygen pressure of 1×10^{-6} mbar in a chamber different from the one used for the deposition of the REN.

One of the MBE systems at the Max Planck Institute for Chemical Physics of Solids (MPI-CPfS) in Germany is equipped with two effusion cells and a leak valve. High purity Ho was evaporated from a LUXEL Radak effusion cell, and the flux rate was measured using a quartz crystal monitor at the growth position. A flux rate of 1 Å/min was typically used. The rare earth was evaporated in the presence of molecular nitrogen, supplied through the leak valve. Most of the rare earths, including Ho, have a catalytic effect that allows a reaction between the rare earth and N_2, spontaneously forming a REN layer [10]. The nitrogen partial pressure P_{N_2} and the substrate temperature T_{sub} were varied for each film. For the optimization procedure, the growth time was fixed at 2 hours, unless otherwise stated.

The samples were characterized *in situ* by reflection high-energy electron diffraction (RHEED) using a STAIB Instruments RH35 system operated at a kinetic energy of 20 keV and by x-ray photoelectron spectroscopy (XPS) using monochromatized Al-K_α light (1486.6 eV) and a Scienta R3000 electron energy analyzer. The XPS spectra were recorded at room temperature in normal emission, with an overall energy resolution of about 0.35 eV. The growth and

in situ characterization are performed under UHV conditions with base pressures of $\approx 1 \times 10^{-10}$ mbar.

The characterization was complemented with *ex situ* structural and magnetic measurements. To prevent a degradation in air, the HoN films were capped *in situ* with 5-20 nm of Cr before being removed from the vacuum system. *Ex situ* x-ray diffraction (XRD) measurements were performed with a PANalytical XPert PRO diffractometer using monochromatic Cu-$K_{\alpha 1}$ radiation ($\lambda = 1.54056$ Å). The magnetic properties of the thin films were measured in a MPMS3 SQUID magnetometer from Quantum Design with a base temperature of 1.8 K and magnetic fields up to 7 T.

X-ray absorption spectroscopy (XAS) measurements were conducted *in situ* at the TPS 45A beamline of the National Synchrotron Radiation Research Center (NSRRC) in Taiwan. The spectra were measured at room temperature in the total electron yield mode. In order to obtain an energy reference for the Ho $M_{4,5}$ and N K edges, the Eu M_5 spectra of EuCoO$_3$ and the Ti $L_{2,3}$ spectra of SrTiO$_3$ were measured simultaneously in a separate chamber. An MBE system similar to the one at the MPI-CPfS is directly connected to the MPI end station, which allows to reproduce the growth of epitaxial HoN films with minimal changes in the growth conditions.

III. RESULTS AND DISCUSSION

A. Growth study of HoN films

HoN films were grown by molecular beam epitaxy on two different substrates, namely MgO (100) and LaAlO$_3$ (100). MgO, similarly to the RENs, crystallizes in the NaCl structure. However, it has a significantly smaller lattice constant of 4.21 Å, which results in a lattice mismatch in relation to HoN of about +15.6%. LAO, on the other hand, has a perovskite structure with a rhombohedral distortion and a pseudocubic lattice parameter of 3.79 Å, yielding a lattice mismatch of –9.1%, when considering a $\sqrt{2}$ factor, i.e., a 45° rotation of the cubic lattice.

For the investigation of the quality of the films on both substrates, we carried out a study consisting of three distinct sets of samples prepared at molecular nitrogen pressures of 1×10^{-7} mbar, 1×10^{-6} mbar and 1×10^{-5} mbar. For each of the series, the substrate temperature was used as a varying parameter. The next two subsections explore the different series by *in situ* characterization using electron diffraction and x-ray photoelectron spectroscopy experiments.

1. HoN on MgO (100)

We start the investigation with the films on MgO (100) substrates grown at a nitrogen pressure of 1×10^{-6} mbar. To study the crystallinity, we performed RHEED measurements. Selected diffraction patterns are shown in Figs. 1(d)–1(f). For the film grown at $T_{sub} = 200$ °C [Fig. 1(d)], we observe a ring-like RHEED pattern with sharper, ordered spots superimposed. This is indicative of a majorly polycrystalline sample with some texturing.

Increasing the substrate temperature to 300 °C [Fig. 1(e)] slightly improves the crystalline structure of the film. Now the ring pattern disappears, and only the transmission spots characteristic of a three-dimensional growth are visible. Since
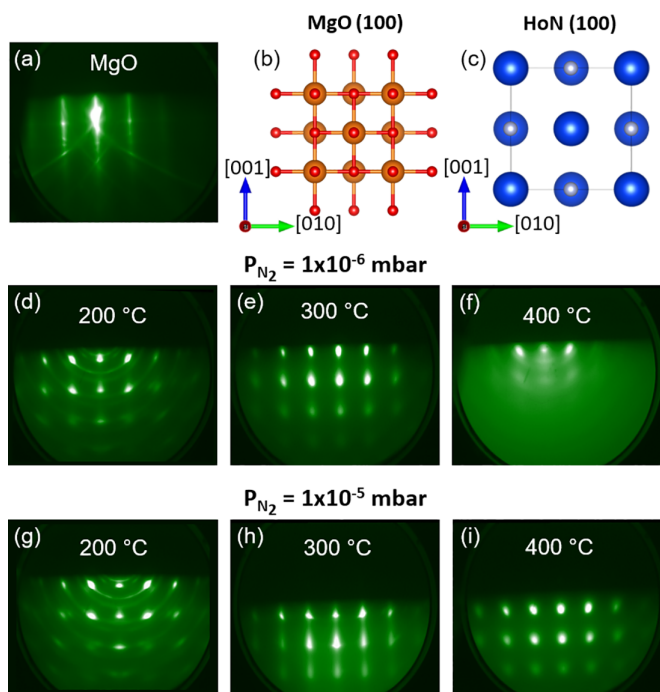
FIG. 1. Selected RHEED pictures of the annealed MgO (100) substrate (a) and the HoN films grown at [(d),(e),(f)] $P_{N_2} = 1 \times 10^{-6}$ mbar and [(g),(h),(i)] $P_{N_2} = 1 \times 10^{-5}$ mbar, at the substrate temperatures indicated in the individual panels. [(b),(c)] Sketches of the crystal structures of substrate and film indicating the in-plane orientation of the (100) surfaces for the acquired RHEED patterns.

MgO (100) has a large lattice mismatch in relation to HoN, island growth and consequent sizable roughness of the film are indeed expected. The crystallinity of this sample is comparable to GdN grown on MgO (100) reported in Ref. [14]. For a substrate temperature of 400 °C [Fig. 1(f)], however, the RHEED pattern is significantly degraded, hinting towards a lower quality of the sample and/or the eventual appearance of extraneous phases.

The composition of the films was then evaluated by XPS measurements. Figure 2 shows the survey spectra of HoN
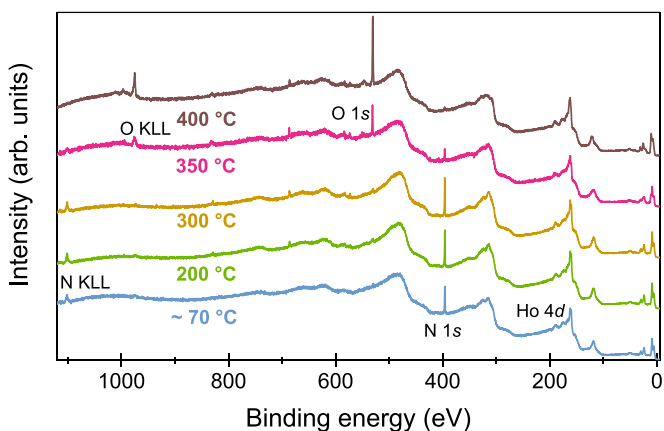

FIG. 2. XPS survey spectra of HoN films grown on MgO (100) at a nitrogen partial pressure of 1×10^{-6} mbar and at various substrate temperatures.
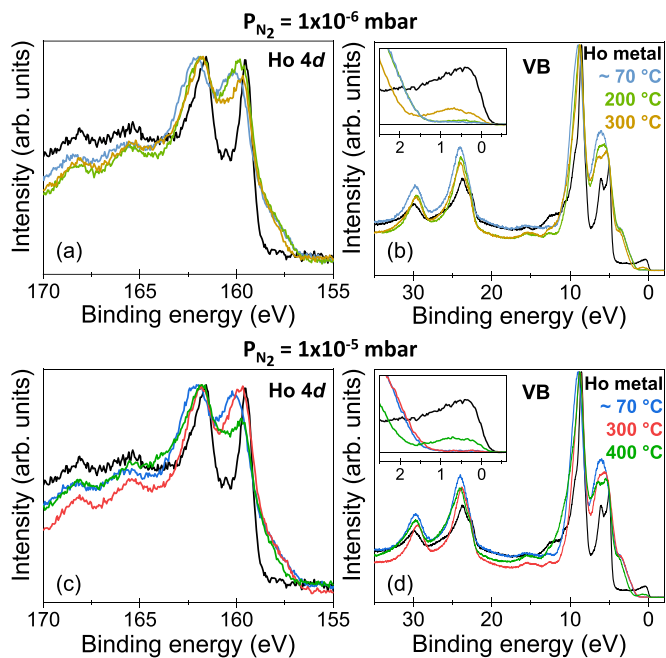

FIG. 3. Ho $4d$ and valence band XPS of HoN films grown on MgO (100) at $P_{N_2} = 1 \times 10^{-6}$ mbar [(a),(b)] and $P_{N_2} = 1 \times 10^{-5}$ mbar [(c),(d)] for various substrate temperatures. Reference spectra of metallic Ho are shown in black. The insets show close ups of the VB spectra for the region near the Fermi level.

grown at a nitrogen partial pressure of 1×10^{-6} mbar and various temperatures up to 400 °C. The lowest temperature (≈ 70 °C) results from the thermal equilibrium between the unheated sample holder and the Ho effusion cell, which was reached several minutes after the growth started. For substrate temperatures ranging from ≈ 70 °C up to 300 °C, all the prominent peaks in the survey spectra are attributed to either holmium or nitrogen, and no major contamination is observable. However, the spectrum is significantly different for $T_{sub} = 350$ °C, where the N $1s$ peak (396 eV) is very reduced, while a peak at 531 eV—attributed to oxygen—gains intensity. The trend continues for $T_{sub} = 400$ °C, where the nitrogen peak almost disappears and the oxygen peak increases further. For high substrate temperatures, oxygen seemingly starts to substitute nitrogen, suggesting a preferred reaction of holmium with oxygen. The formation of a holmium oxide phase could then also explain the disordered RHEED observed in Fig. 1(f). The contamination is likely caused by a reaction with the oxide substrate, facilitated by the higher temperatures. This is discussed in more detail in Appendix A and Fig. 10.

To further investigate the quality of the HoN films, we measured the Ho $4d$ core level and valence band (VB) spectra for three films grown at 1×10^{-6} mbar of nitrogen for which no significant oxygen contamination is observed. These are shown in Figs. 3(a) and 3(b), together with the respective spectra of metallic holmium as reference (in black). The Ho $4d$ spectra were normalized to the height of the peak at around 162 eV, while the valence band spectra were normalized to the intensity at around 8.7 eV. The XPS spectra of the film grown at the lowest temperature (in light blue) show clear differences

from that of metallic holmium. The Ho $4d$ peaks are broader in the nitride and, in the case of the valence band, where the Ho $4f$ states ($\approx$5–10 eV) are predominant, the peak at $\approx$7 eV has higher relative intensity and loses the double peak shape present in the metal. Moreover, a distinct peak at about 3 eV is now observed. The N $2p$ states are expected to appear in that energy range, according to previous XPS and x-ray emission measurements [8]. In addition, the intensity near the Fermi level ($\approx$0.5 eV) is almost completely suppressed in the nitride film. For the film grown at 200 °C (light green), the peak at $\approx$7 eV still has a similar broad character, albeit with a decreased intensity. The intensity near the Fermi level is still low. As the substrate temperature increases to 300 °C, some alterations are noticeable. Namely, the Ho $4d$ peak at $\approx$160 eV decreases in intensity and becomes narrower, while the valence band peak at $\approx$7 eV recovers the double peak feature, thus becoming closer to the spectrum of metallic holmium. Moreover, the peak close to the Fermi level gains intensity and is quite pronounced for the film grown at this higher temperature.

We now direct our attention to the series of films grown at $P_{N_2} = 1 \times 10^{-5}$ mbar. For these, the RHEED patterns show no signs of degradation for substrate temperatures of up to 400 °C, the highest temperature used, as can be confirmed in Figs. 1(g)–1(i). The RHEED patterns look overall similar to the previous series, but for 300 °C the pattern shows more elongated spots forming faint streaks, suggesting a better crystalline structure for that film.

The XPS survey spectra of this set of samples (not shown) indicate no significant incorporation of oxygen up to $T_{sub} = 400$ °C, in contrast to the observations on the lower pressure series. The higher nitrogen pressures used during the growth therefore allow a larger tolerance in the choice of the substrate temperature without the unwanted reaction between the rare earth and the oxide substrate. Nevertheless, for the highest substrate temperature, some alterations of the valence band and Ho $4d$ spectra are observed, see Figs. 3(c) and 3(d). Similarly to what happens for the series grown at $P_{N_2} = 1 \times 10^{-6}$ mbar, when the temperature of the substrate increases substantially, the peak at 160 eV decreases in intensity, while the peak at $\approx$7 eV gains a clear double feature and the intensity at $\approx$0.5 eV increases significantly.

A third series of films was grown at low nitrogen pressures of 1×10^{-7} mbar. For these, the XPS measurements show the presence of metallic holmium even at the lowest substrate temperature (not shown here). At a substrate temperature of 200 °C, XPS shows Ho features closer to the metal, and the survey spectrum indicates that some oxygen contamination is already present. The nitrogen partial pressure may not be sufficient to entirely react with the rare earth, resulting in large amounts of metallic clusters being present in these films. The low nitrogen pressure also favors the preferred reaction of Ho with oxygen at lower substrate temperatures than for the higher pressure series.

2. HoN on LaAlO$_3$ (100)

A similar growth study was performed on LaAlO$_3$ (100) substrates. In Figs. 4(d)–4(f) we show a selection of RHEED patterns of HoN films grown at $P_{N_2} = 1 \times 10^{-6}$ mbar. For
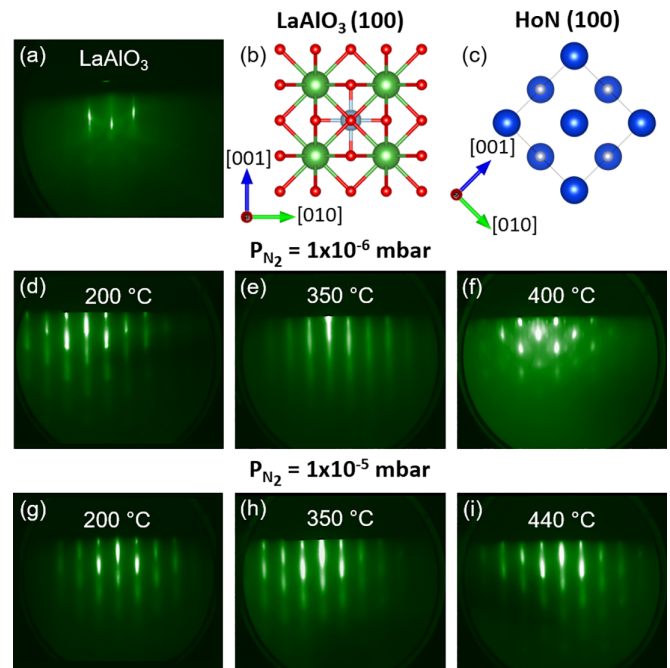

FIG. 4. Selected RHEED pictures of the annealed LaAlO$_3$ (100) substrate (a) and the HoN films grown at [(d),(e),(f)] $P_{N_2} = 1 \times 10^{-6}$ mbar and [(g),(h),(i)] $P_{N_2} = 1 \times 10^{-5}$ mbar, at the substrate temperatures indicated in the individual panels. [(b),(c)] Sketches of the crystal structures of substrate and film indicating the in-plane orientation of the (100) surfaces for the acquired RHEED patterns.

substrate temperatures of 200 and 350 °C they show well-defined streaks, albeit with some intensity modulation especially for the lower substrate temperature, characteristic of a moderately rough surface. This is in contrast to the observations for the films grown on MgO substrates [cf. Figs. 1(d) and 1(e)], where a polycrystalline/island growth was observed. Moreover, the lattice constant calculated from the spacing of the RHEED streaks matches, within the error, the expected value for HoN with a 45° rotation in relation to the LAO (100) surface. Despite the considerably high lattice mismatch, HoN seems to have a relatively well-ordered growth on LAO substrates.

Similarly to what happens for the same conditions on MgO, when $T_{sub} = 400$ °C was used, the RHEED pattern shows signs of degradation [see Fig. 4(f)].

The films were once again characterized by XPS. Figure 5(a) shows the survey spectra of the films grown at $P_{N_2} = 1 \times 10^{-6}$ mbar. For substrate temperatures up to 350 °C all the peaks belong to nitrogen or holmium. It is worth noting the difference between the spectra of the films grown at $P_{N_2} = 1 \times 10^{-6}$ mbar and $T_{sub} = 350$ °C for the different substrates [pink curves in Figs. 2 and 5(a)]. When LAO is used as a substrate no oxygen contamination is observed for these growth conditions. Nonetheless, by increasing T_{sub} to 400 °C, we still observe a similar behavior where the nitrogen peak decreases and the oxygen peak gains intensity. This indicates that it is possible to grow HoN at higher substrate temperatures on LAO than on MgO. But, given a sufficiently high T_{sub}, oxygen from the substrate is still reacting with the rare earth.
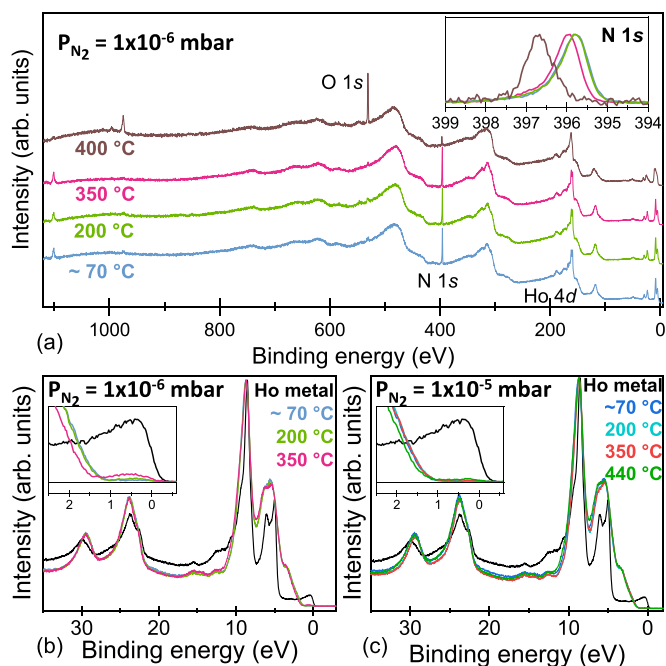
FIG. 5. (a) XPS survey spectra of HoN films grown on LaAlO$_3$ (100) at a partial nitrogen pressure of 1×10^{-6} mbar and substrate temperatures ranging from $\approx$70 °C to 400 °C. The inset shows the N 1s core levels normalized to the peak height. [(b),(c)] Valence band XPS for the films grown at P$_{N_2}$ = 1×10^{-6} mbar (b) and P$_{N_2}$ = 1×10^{-5} mbar (c) on LAO. The insets show close ups of the region near the Fermi level.

The Ho 4d spectra are now very similar across the entire series, except for T$_{sub}$ = 400 °C, and they look identical to those of the films grown on MgO at T$_{sub}$ = 200 °C and P$_{N_2}$ = 1×10^{-6} mbar, and T$_{sub}$ = 300 °C and P$_{N_2}$ = 1×10^{-5} mbar [cf. green curve in Fig. 3(a) and red curve in Fig. 3(c), respectively]. While the differences in the Ho 4d are much more subtle for the films grown on LAO, some differences can be observed in other regions. The inset in Fig. 5(a) shows the N 1s for the same films, normalized to the peak height. It is noticeable that the peak shifts to higher binding energies as the substrate temperature increases, with quite a significant shift for the high temperature film with oxygen contamination. The valence band region, shown in Fig. 5(b), also shows some changes across the series. The Ho 4f peak at $\approx$7 eV has a smaller change than in the previous section, but a tendency towards a double peak feature is still visible for the highest substrate temperature where only the nitride is present (T$_{sub}$ = 350 °C). Furthermore, the intensity near the Fermi level hardly changes for substrate temperatures of up to 200 °C. For higher temperatures the intensity gradually increases.

For the films grown at the highest nitrogen pressure on LAO, RHEED measurements shown in Figs. 4(g)–4(i) suggest that the crystallinity of the films is comparable to the series with P$_{N_2}$ = 1×10^{-6} mbar, with a modulated streaky pattern. In contrast, however, there are now no signs of degradation even at T$_{sub}$ = 440 °C. Furthermore, XPS measurements do not show any significant oxygen contamination for the entire range of substrate temperatures nor notable differences in the N 1s and Ho 4d core levels. The valence band XPS
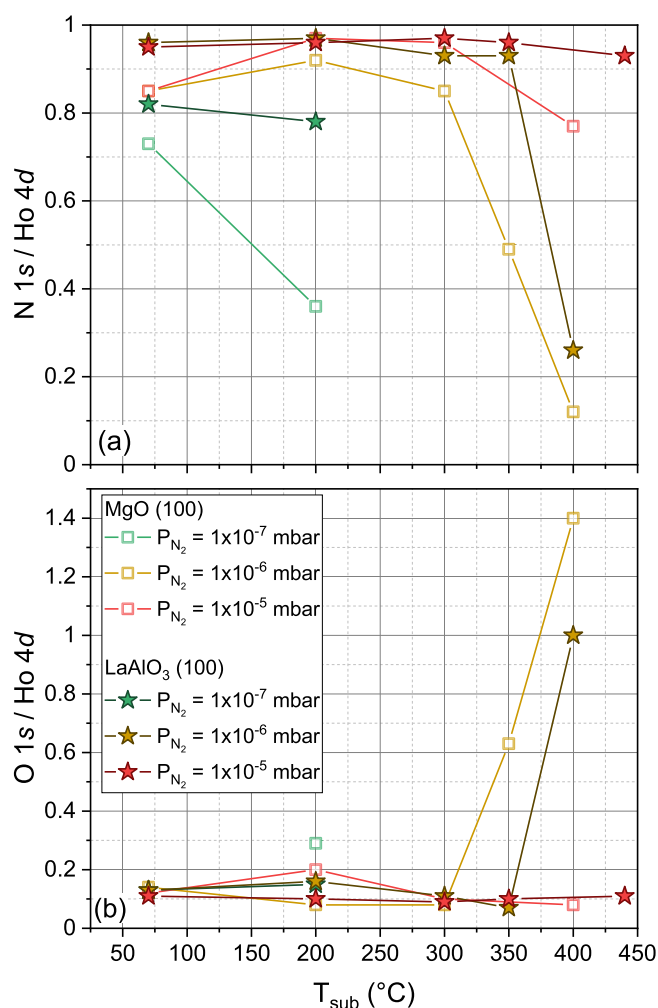

FIG. 6. N 1s/ Ho 4d (a) and O 1s/ Ho 4d (b) ratios calculated from the integrated intensities of the corresponding XPS core levels.

spectra, illustrated in Fig. 5(c), show some subtle changes, especially for the film grown at 440 °C. Here the intensity near the Fermi level is slightly higher than for lower substrate temperatures; however the region still has a reduced intensity when compared to the films grown at high temperature and at lower nitrogen pressure. This suggests that the films grown at P$_{N_2}$ = 1×10^{-5} mbar on LAO are more robust to temperature variations, with only minimal changes detected by RHEED and XPS across the series.

3. XPS evaluation of the nitrogen content

A more quantitative interpretation of the composition and growth window of HoN can be obtained from the relative integrated intensities of the Ho 4d and N 1s core levels. A description of the analysis procedure, using Ho$_2$O$_3$ as a reference, can be found in Appendix B and Fig. 12. The ratios are shown in Fig. 6(a) for all the films grown on MgO (open squares) and LAO (filled stars) substrates. Although this cannot be taken as an absolute indicator of the stoichiometry of the samples due to systematic errors in the determination of the integrated intensities, analyzer efficiency, and photoionization cross sections, as well as possible differ-

ences in the composition of the bulk and surface, it still is a valuable tool to understand how the nitrogen pressure and the substrate temperature affect the nitrogen content in the films. Additionally, Fig. 6(b) shows the O 1s/ Ho 4d ratios in order to study the oxygen contamination of the different series of films. In this regard, it is worth noting that a small amount of oxygen is always present in the films. Values between 0.1–0.2 result from a slow degradation of the samples over the course of the XPS measurement, even under UHV conditions. This is discussed in more detail in Appendix A and Fig. 11.

For the case of the films grown on MgO (100) at the lowest nitrogen pressure of 1×10^{-7} mbar (green squares), the nitrogen content is quite far below the ideal value (1) even at the lowest substrate temperature. This suggests that the low nitrogen pressure may not be sufficient to entirely react with the rare earth. By increasing the substrate temperature to 200 °C the nitrogen content decreases very rapidly and this is accompanied by an increase of the oxygen content to values above the baseline. For the films grown at $P_{N_2} = 1 \times 10^{-6}$ mbar (yellow squares) and $P_{N_2} = 1 \times 10^{-5}$ mbar (red squares), the nitrogen content is relatively reduced for the lowest substrate temperature, albeit higher than for the lower pressure sample, and it reaches its maximum at 200 °C (for $P_{N_2} = 1 \times 10^{-6}$ mbar) or 200–300 °C (for $P_{N_2} = 1 \times 10^{-5}$ mbar). The nitrogen content then decreases slightly at 300 °C for $P_{N_2} = 1 \times 10^{-6}$ mbar and at 400 °C for $P_{N_2} = 1 \times 10^{-5}$ mbar. This reduction coincides with the changes in the Ho 4d and especially in the valence band discussed in Sec. III A 1 (see Fig. 3). The intensity of the peak at ≈ 0.5 eV increases for these conditions, and the appearance of this feature can therefore be taken as a qualitative indicator of a decreasing nitrogen content in the samples. Upon further increase of the substrate temperature, the nitrogen content is drastically reduced, coinciding with the sudden increase in the oxygen ratio observable in Fig. 6(b) resulting from the undesirable reaction between holmium and the oxide substrate.

As for the films grown on LAO one can observe that the lowest nitrogen pressure of 1×10^{-7} mbar (green stars) allows the growth of films with higher nitrogen content than the equivalent series on MgO, although the values still deviate quite far from the ideal. For 1×10^{-6} mbar (yellow stars) the nitrogen ratio is the highest for substrate temperatures of ≈ 70 °C and 200 °C, and has a small decrease for 300 °C and 350 °C. The reduction happens when the feature near the Fermi level starts to gain intensity, and the N 1s peak shifts to higher binding energies, as can be verified in Figs. 5(a) and 5(b). By further increasing the substrate temperature, the nitrogen is eventually suppressed and the oxygen increases, similarly to what was observed on MgO. For the series grown at the highest nitrogen pressure (red stars) the nitrogen ratio is relatively constant and close to 1 when the substrate temperature is kept within the range 70–350 °C. For the highest temperature nitrogen is slightly suppressed, in accordance with the small changes observed in the VB [Fig. 5(c)].

From these results it is apparent that, for a given, sufficiently high, nitrogen pressure, the N 1s/Ho 4d ratios have nearly the ideal value for a larger temperature range when the substrate is LAO. Overall this indicates that the growth of HoN is more robust on LAO, which results in a larger growth window. Furthermore one can observe that, for temperatures

above a certain threshold (that varies with the nitrogen pressure and substrate), the nitrogen content invariably decreases before the rare earth starts to react with oxygen. This evolution suggests that the higher substrate temperatures favor the incorporation of less nitrogen in the films. This has been reported for other REN thin films [5,19,30,40], and is usually attributed to the formation of nitrogen vacancies.

From the combined study of RHEED and XPS one can infer the growth conditions necessary to obtain HoN films with good quality. Firstly, LAO substrates should be used in order to guarantee films with a relatively good crystalline structure. Moreover, nitrogen pressures of 1×10^{-5} mbar and substrate temperatures between 200 and 350 °C were identified as the best parameters and were used for further characterization of the optimized HoN films.

B. Structural, electronic, and magnetic properties of epitaxial HoN

Further investigation of the structural properties of the films was carried out with x-ray diffraction (XRD). Figure 7(a) shows the XRD scan of an optimized film with high nitrogen content and a growth time of 4 hours. The sample was capped with 5 nm of Cr prior to removing it from the UHV system. All peaks in the XRD scan are attributed to either the substrate or the (2n 0 0) family of planes expected for HoN, and no parasitic phases are observed. XRD yields a lattice parameter of 4.874 ± 0.003 Å, in good agreement with experimental values reported previously [8,9,35]. Figure 7(b) shows the in-plane ϕ scan of the HoN (111) reflection (in black), with a fourfold set of peaks, and with a shift of 45° with respect to the LaAlO$_3$ substrate (in gray). The measurement thus confirms the epitaxial relationship between the rare-earth nitride and the pseudocubic LAO substrate that had already been observed by RHEED. In addition, x-ray reflectivity (XRR) was measured and is shown in Fig. 7(c). From the period of the interference fringes, one can determine the thickness of the HoN film, which was found to be approximately 32 nm. This indicates a thin film growth rate of about 1.3 Å/min. Moreover, the decay rate of the intensity of the fringes with increasing angle suggests an upper limit of around 5 Å for the roughness of the HoN layer.

To gain information about the electronic structure of the HoN thin films and to evaluate the valence of the rare-earth ion, we performed *in situ* x-ray absorption spectroscopy experiments at the Ho $M_{4,5}$ edges and N K edge. The $M_{4,5}$ absorption edges probe the $3d^{10} 4f^n \rightarrow 3d^9 4f^{n+1}$ dipole-allowed multiplet transitions of the rare earth. Figure 8(a) shows the spectra of three HoN films with different nitrogen contents, as determined by XPS. The film whose spectrum is shown in blue has the highest nitrogen content. In green is the XAS of a film with about 20% less nitrogen than the previous sample. The third film, in orange, has a very large nitrogen deficiency with about 55% less nitrogen than the optimized sample and it already contains metallic Ho clusters. In addition, we show a holmium metal reference film in black. When comparing the spectra of the nitride films and of the metal one cannot identify any differences. The results are also similar to the HoN films reported by Brown *et al.* [8], and to the Ho^{3+}-compound Ho$_2$O$_3$ [41]. Moreover, the experimental line
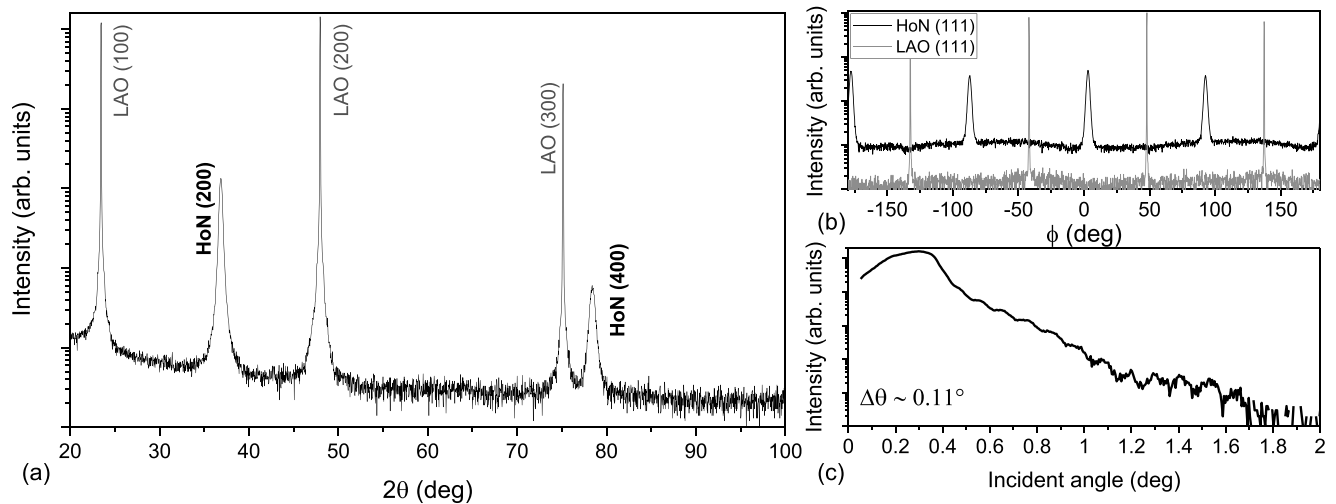
FIG. 7. XRD $\theta - 2\theta$ scan (a), in-plane ϕ scan (b) and XRR curve (c) of HoN grown on LaAlO$_3$ (100) for 4 hours at 350 °C and $P_{N_2} = 1 \times 10^{-5}$ mbar. The film was capped *in situ* with 5 nm of Cr.

shapes are in agreement with atomic multiplet calculations for a $4f^{10}$ configuration [8,42]. These observations confirm, on the one hand, that the $4f$ states in HoN are localized and atomic-like and, on the other hand, that the holmium ions have a stable trivalent state for all the films, independently of their nitrogen content.

The N K edge provides information about the p-projected partial density of states of the conduction band. The measurements are presented in Fig. 8(b) for the same HoN samples. The two main peaks in the spectra of the samples without metallic clusters, at 400 and 405 eV, have been associated with the rare earth 5d t_{2g} and e_g states, respectively [16]. For the film with high nitrogen content the overall shape and features of the spectrum look similar to earlier studies on the same material [8] and other rare-earth nitrides [5,16]. Nonetheless, the low-energy shoulder at $\approx$398 eV is much less pronounced for our films and the splitting between the main peaks is larger in the current experiment, when compared to

the report of Brown *et al.* [8]. Furthermore, and in opposition to the Ho $M_{4,5}$-edges, the N K-edge spectra of the films now show some differences depending on the composition. In fact, for lower nitrogen content (in green), a new feature starts to appear in between the two main peaks, at a photon energy of approximately 403 eV. For the film with metallic clusters large changes are observed. The intensity of the peak at 405 eV is significantly reduced, while the peak at 403 eV gains intensity, and the peaks at 400 and 410 eV are shifted to lower energies, in agreement with the more metallic character.

We finally discuss the magnetic properties of an optimized HoN film, investigated by SQUID magnetometry. The film was grown on LAO at 350 °C and $P_{N_2} = 1 \times 10^{-5}$ mbar for 4 hours and was capped *in situ* with 20 nm of Cr to avoid oxidation when exposed to air. The background signals of the sample holder, substrate, and Cr capping layer were subtracted for all the measurements, and the data presented here should therefore have the contribution of the HoN layer only. The routine for the background correction applied to the magnetization data is described in Appendix C. Furthermore, the thickness obtained from XRR measurements was used to estimate the magnetization in Bohr magnetons per Ho ion.

Figure 9(a) shows the temperature-dependent magnetization curves of the film, measured after cooling in magnetic fields of 0.001 T, 0.01 T, 0.1 T, and 1 T parallel to the sample plane. We additionally show neutron diffraction data from a polycrystalline HoN bulk sample [35], and magnetization data measured at an applied magnetic field of 1 T for bulk [38] and thin film [9] samples.

For the present study, we observe that the magnetization increases with decreasing temperature for all the applied magnetic fields. Moreover, and except for a field of 1 T, there is a distinct separation between field cooled and zero-field cooled measurements, as shown exemplarily for the lowest magnetic field in Fig. 9(b), indicating a clearly predominant ferromagnetic component in the sample.

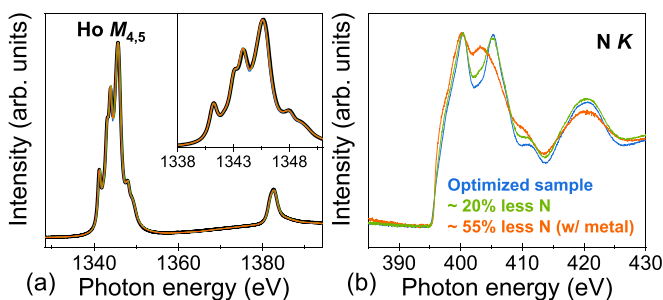In the low-field limit, the transition is nicely shaped with a Curie temperature of about 27 K, as determined

FIG. 8. Holmium $M_{4,5}$-edges (a) and nitrogen K-edge (b) x-ray absorption spectra of three HoN films with varying nitrogen content. All the films were grown at a substrate temperature of 250 °C. The optimized film (in blue) was grown at $P_{N_2} = 1 \times 10^{-5}$ mbar, the sample with $\approx$20% less nitrogen (in green) was grown at $P_{N_2} = 1 \times 10^{-6}$ mbar, and the film with $\approx$55% less nitrogen and Ho clusters (in orange) was grown at $P_{N_2} = 5 \times 10^{-7}$ mbar. A spectrum of metallic holmium is included in black in panel (a) for comparison. All the spectra were normalized to their maximum intensity.
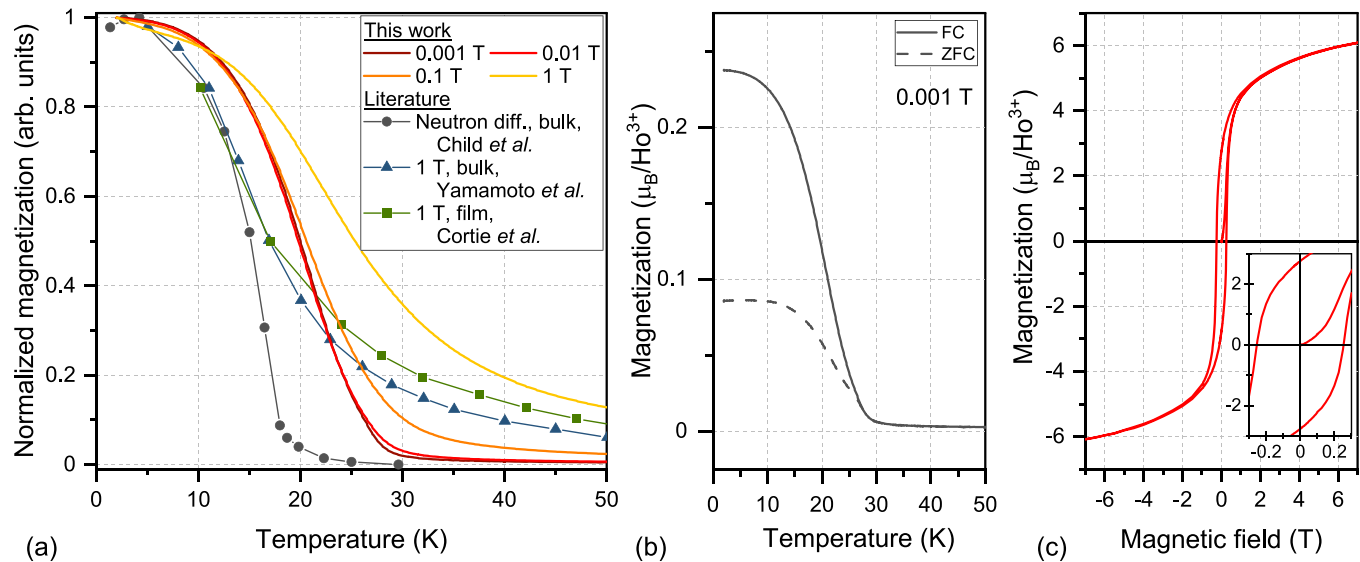
FIG. 9. (a) Normalized magnetization as a function of temperature of a HoN film grown at $T_{sub} = 350\,°C$, $P_{N_2} = 1 \times 10^{-5}$ mbar for 4 hours and capped *in situ* with 20 nm of Cr. The sample was measured in field cooled conditions with applied magnetic fields of 0.001 T, 0.01 T, 0.1 T, and 1 T. Experimental data from Child *et al.* [35], Yamamoto *et al.* [38] and Cortie *et al.* [9] are shown for comparison. (b) Field cooled (FC) and zero-field cooled (ZFC) measurements at an applied magnetic field of 0.001 T. (c) Field dependence of the magnetization at 2 K for the same film, with a close-up of the low-field region in the inset.

by a linear extrapolation of the magnetization to zero. By increasing the applied magnetic field, we observe a smearing of the transition. From the direct comparison between our low-field measurements and the neutron diffraction data [35] shown in gray circles, we observe that the curves are similarly shaped, but the previous experiment has a significantly lower ordering temperature. In fact, the value observed in our study is higher than the commonly reported values in the literature that generally vary between 13 and 18 K [35,37,38].

The relatively steep transition observed in our sample, well defined for 0.001 T, contrasts with some of the previous results on HoN thin films [9] and bulk samples [38], where the magnetic response in low magnetic fields is very small, and only for higher fields some increase of the magnetization is observed for lower temperatures [cf. green squares and blue triangles in Fig. 9(a)]. Our results are consistent with the expected predominant ferromagnetic behavior of HoN, revealing a good quality of the sample.

The magnetic hysteresis loop measured at a temperature of 2 K is shown in Fig. 9(c) for the same film. The magnetic moment measured at 7 T is approximately 6 μ_B/Ho^{3+}. Comparing the measurement results of various HoN thin films, we can give an estimate of the accuracy of the magnetic moment at 7 T to be around ± 1 μ_B/Ho^{3+}, which is related to uncertainties in the determination of the thickness and area of the sample. Our measured value of about 6 μ_B/Ho^{3+} is significantly higher than observed in previous thin film experiments [9] and close to the range of the saturation values reported in bulk neutron diffraction measurements on polycrystalline samples [35] and magnetization on single crystals [39]. Nevertheless, and as usually reported, the ordered magnetic moment is smaller than the 10 μ_B associated with the Ho^{3+} ion, which is commonly attributed to complex spin structures or a partial

quenching of the orbital moment induced by crystal field interactions [9,35,36,39].

Here we would like to note that some of our M(H) measurements have a slope at high magnetic fields that might be caused by the error introduced by the subtraction of the relatively large background, which has a majorly linear behavior in high fields. Because of that it is difficult to unequivocally determine whether a saturation of the magnetization has been reached at 7 T.

The coercive field is approximately 250 mT at 2 K, as can be observed in the inset of Fig. 9(c), and decreases to $\approx$200 mT at 5 K, which is more than one order of magnitude larger than the reported by Cortie *et al.* [9] and our films seem magnetically less soft than those in the previous study.

Additionally, we observed that changes of a few percent in the nitrogen content have an effect on the magnetic properties of the samples, as the magnetic ordering temperature decreases with increasing nitrogen deficiency. A decrease of $\approx$3 K was found for a sample with $\approx$4% less nitrogen. This suggests that samples with lower Curie temperature suffer from nonstoichiometry. Nevertheless, the moment measured at high fields does not change significantly indicating that the moment is largely determined by the 4f configuration of the rare earth, which is robust against relatively small changes in the nitrogen content. A similar observation has been reported for thin films of DyN [11].

IV. CONCLUSIONS

We have successfully grown (100)-oriented HoN on MgO and LAO substrates by MBE under UHV and mild temperature conditions, and demonstrated that the nitrogen content of the samples can be controlled through the variation of the substrate temperature and nitrogen pressure. The films grow

epitaxially on the two substrates, as confirmed by XRD and/or RHEED. Nevertheless, the substrate choice has a notable influence on the growth window and structural quality of the samples. We have found that the films grown on MgO are significantly rough due to the large lattice mismatch between the nitride and the substrate, while a more robust and well-ordered growth happens on LAO.

X-ray absorption spectroscopy on the Ho $M_{4,5}$ edges confirmed the trivalent state of the holmium ions independently of the composition of the samples.

The magnetic properties of an optimized HoN sample were studied, and we have found a nicely shaped magnetization curve yielding a Curie temperature of about 27 K, which is 50% higher than previously observed. The measured magnetic moment at 7 T is in agreement with reports on bulk samples, and lower than predicted for the Ho^{3+} ion, which may be related to a complex magnetic structure or a partial quenching of the orbital moment caused by crystal field effects. Future measurements at higher magnetic fields could provide more insights into this open question.

ACKNOWLEDGMENTS

APPENDIX A: ORIGIN OF THE OXYGEN CONTAMINATION IN HoN FILMS

We return here to the topic of the oxygen contamination discussed in the main text. We have observed that, when growing HoN on both LAO and MgO at temperatures above $350-400\,°C$ and pressures of 1×10^{-6} mbar of nitrogen, large quantities of oxygen were present in the XPS measurements. Two representative spectra illustrating the issue are shown in Fig. 10 in gray and red for the two oxide substrates. In order to investigate the origin of this contamination, we have prepared a film under the same conditions on a metallic Cr layer, shown in blue. For the samples grown on MgO and LAO substrates, we see that the oxygen becomes prevalent, in detriment of nitrogen, indicating the formation of HoO_x. On the other hand, when a film is grown at the same conditions on metallic Cr, only a very small oxygen peak is observed. This indicates that the oxygen is likely being provided by the substrate when heated to relatively high temperatures.

For the remaining films, grown at lower substrate temperatures and/or higher nitrogen pressures, no significant parasitic phase of holmium oxide is formed. However, a small oxygen peak is still always observable. Figure 11 shows the O 1s peak for HoN grown at $P_{N_2} = 1\times10^{-5}$ mbar and $T_{sub} = 200\,°C$ on an oxide substrate (LAO) on the left and a nonoxide substrate (Cr) on the right. In both cases we show the first measurement iteration, taken some minutes after growth, and
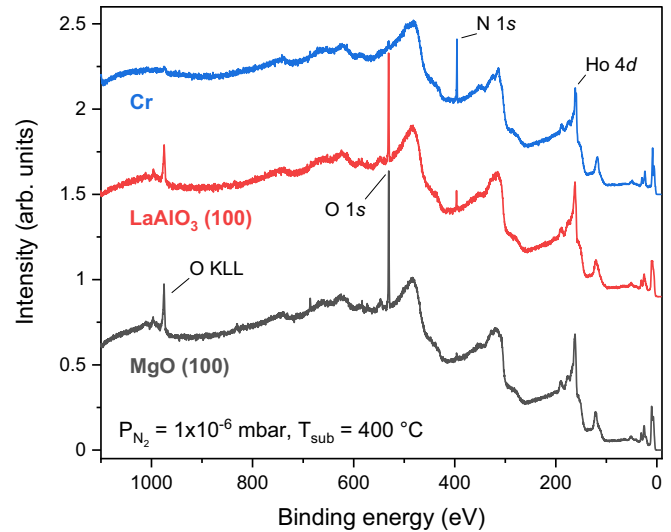

FIG. 10. XPS survey spectra of HoN films grown under the same conditions ($T_{sub} = 400\,°C$, $P_{N_2} = 1\times10^{-6}$ mbar) on oxide substrates MgO (100) in gray and LaAlO$_3$ (100) in red and a nonoxide substrate Cr in blue.

the last iteration, approximately 20 hours after the growth. The sum of all the iterations is also shown in red. For both substrates the amount of oxygen in the first measurement iteration is negligible at the lower temperatures. The O 1s peak rather increases with time. This suggests that, in this case, the small oxygen contamination does not come from the substrate nor is it incorporated during the growth. In fact, it appears to come from the environment of the measurement chamber, despite the UHV conditions with pressures of about 2×10^{-10} mbar.

APPENDIX B: DETERMINATION OF N/Ho AND O/Ho RATIOS

In order to gain quantitative information about the composition of the samples, we calculated the relative concentrations
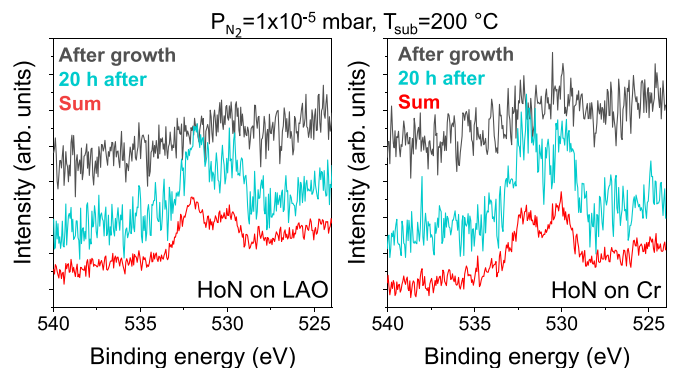

FIG. 11. O 1s spectra of HoN films grown under the same conditions ($T_{sub} = 200\,°C$, $P_{N_2} = 1\times10^{-5}$ mbar) on LaAlO$_3$ (100) (left) and on Cr (right). The first measurement iteration, taken immediately after the growth, is shown in gray. In blue is the spectrum taken at the end of the entire XPS measurement sequence, approximately 20 h after growth. The sum of all the iterations is shown in red. The spectra were shifted vertically for clarity.
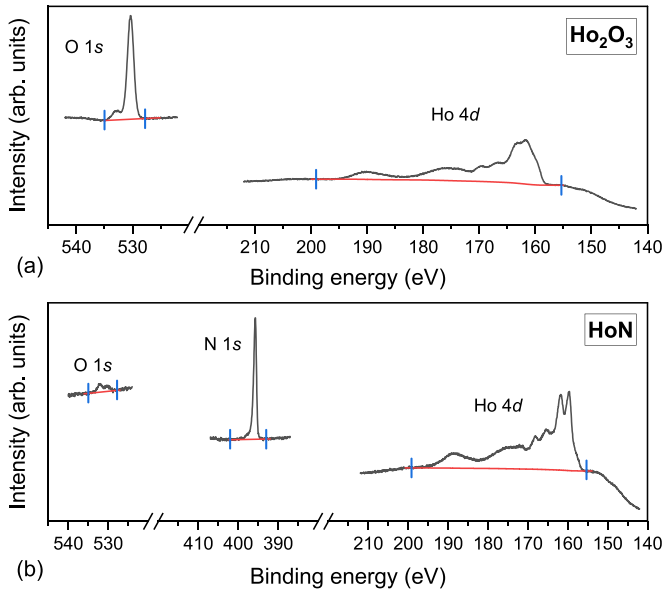
FIG. 12. (a) O 1s and Ho 4d XPS spectra of a Ho$_2$O$_3$ film, used as a reference for the integration ranges. (b) O 1s, N 1s, and Ho 4d XPS spectra of HoN grown on LaAlO$_3$ (100) at T$_{sub}$ = 350 °C and P$_{N_2}$ = 1×10^{-5} mbar. The subtracted backgrounds are shown in red and the integration ranges are indicated in blue.

of their constituents from the XPS core levels. We used a holmium oxide sample as a reference, aiming to reduce the systematic errors associated with the technique.

For this purpose, Ho was evaporated at 1 Å/min in P$_{O_2}$ = 5×10^{-6} mbar at room temperature on metallic Cr, forming Ho$_2$O$_3$. The Ho 4d and O 1s XPS spectra were measured, as illustrated in Fig. 12(a) and a background, shown in red, was subtracted from each of the core levels. For Ho 4d, a Shirley (integral type) background was used, while for O 1s a linear background was preferred due to the sloping background. We calculated the integrated intensities of the core levels from the peak areas in the energy regions indicated by the blue markers, and divided them by the respective photoionization cross sections according to reference [43] (0.1646 Mb for Ho 4d and 0.0400 Mb for O 1s). The integration ranges of Ho 4d and O 1s were chosen such that the ratio O 1s/Ho 4d ≈ 3/2 was obtained, thereby minimizing the systematic errors mentioned in Sec. III A 3.

We then measured the Ho 4d, N 1s, and O 1s XPS spectra for the HoN films, shown in Fig. 12(b). In order to calculate the O 1s/Ho 4d ratios discussed in Fig. 6(b), we used the same background subtraction and fixed energy regions as for the oxide. Regarding the N 1s/Ho 4d ratios discussed in Fig. 6(a), we used the same energy range to calculate the Ho 4d peak area. For the N 1s, we adopt the procedure from the O 1s, since the core levels have a similar shape and relatively close energy position. A linear background was subtracted and the integrated intensity was corrected using the corresponding photoionization cross section of 0.0240 Mb.
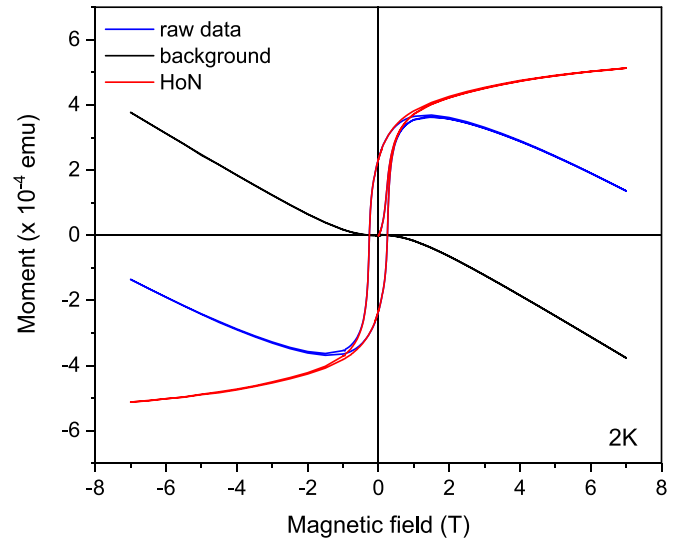

FIG. 13. Hysteresis curve at 2 K of the HoN film shown in Fig. 9 including raw data (LAO substrate + HoN + 20 nm Cr + sample holder, blue), background (reference measurement of LAO substrate + 20 nm Cr + sample holder, black), and extracted HoN contribution (raw data - background, red).

APPENDIX C: BACKGROUND CORRECTION OF THE MAGNETIZATION DATA

Figures 13 and 14 illustrate the treatment of the magnetization data. To derive the HoN contribution, the background signal, which was determined by a reference measurement of the sample holder and a Cr-covered LaAlO$_3$ substrate, was subtracted from the raw data.
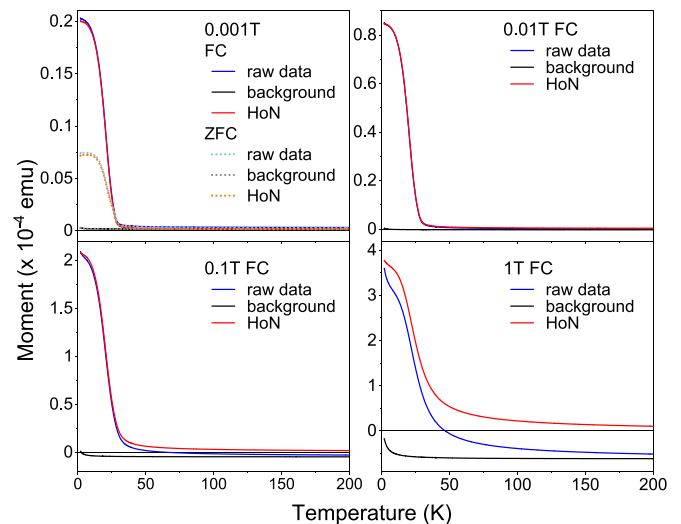

FIG. 14. Field cooled (FC) [and zero-field cooled (ZFC)] temperature-dependent magnetization curves for various magnetic fields of 0.001 T, 0.01 T, 0.1 T, and 1 T of the HoN film shown in Fig. 9 including raw data, background, and extracted HoN contribution.

[1] K. Senapati, M. G. Blamire, and Z. H. Barber, Spin-filter Josephson junctions, Nat. Mater. **10**, 849 (2011).

[2] H. Warring, H. J. Trodahl, N. O. V. Plank, F. Natali, S. Granville, and B. J. Ruck, Magnetic tunnel junctions incorporating a near-zero-moment ferromagnetic semiconductor, Phys. Rev. Appl. **6**, 044002 (2016).

[3] R. Caruso, D. Massarotti, G. Campagnano, A. Pal, H. G. Ahmad, P. Lucignano, M. Eschrig, M. G. Blamire, and F. Tafuri, Tuning of magnetic activity in spin-filter Josephson junctions towards spin-triplet transport, Phys. Rev. Lett. **122**, 047002 (2019).

[4] J. D. Miller, F. H. Ullstad, H. J. Trodahl, B. J. Ruck, and F. Natali, Vertical transport and tunnelling in rare-earth nitride heterostructures, Nanotechnology **31**, 235202 (2020).

[5] F. Natali, B. Ruck, N. Plank, H. Trodahl, S. Granville, C. Meyer, and W. Lambrecht, Rare-earth mononitrides, Prog. Mater. Sci. **58**, 1316 (2013).

[6] S. Granville, B. J. Ruck, F. Budde, A. Koo, D. J. Pringle, F. Kuchler, A. R. H. Preston, D. H. Housden, N. Lund, A. Bittar, G. V. M. Williams, and H. J. Trodahl, Semiconducting ground state of GdN thin films, Phys. Rev. B **73**, 235335 (2006).

[7] C. Meyer, B. J. Ruck, J. Zhong, S. Granville, A. R. H. Preston, G. V. M. Williams, and H. J. Trodahl, Near-zero-moment ferromagnetism in the semiconductor SmN, Phys. Rev. B **78**, 174406 (2008).

[8] J. D. Brown, J. E. Downes, C. J. McMahon, B. C. C. Cowie, A. Tadich, L. Thomsen, J. H. Guo, and P. A. Glans, $p-f$ hybridization in the ferromagnetic semiconductor HoN, Appl. Phys. Lett. **100**, 072108 (2012).

[9] D. L. Cortie, J. D. Brown, S. Brück, T. Saerbeck, J. P. Evans, H. Fritzsche, X. L. Wang, J. E. Downes, and F. Klose, Intrinsic reduction of the ordered $4f$ magnetic moments in semiconducting rare-earth nitride thin films: DyN, ErN, and HoN, Phys. Rev. B **89**, 064424 (2014).

[10] F. Ullstad, G. Bioletti, J. R. Chan, A. Proust, C. Bodin, B. J. Ruck, J. Trodahl, and F. Natali, Breaking molecular nitrogen under mild conditions with an atomically clean lanthanide surface, ACS Omega **4**, 5950 (2019).

[11] W. F. Holmes-Hewett, C. Pot, R. G. Buckley, A. Koo, B. J. Ruck, F. Natali, A. Shaib, J. D. Miller, and H. J. Trodahl, Nitrogen vacancies and carrier-concentration control in rare-earth nitrides, Appl. Phys. Lett. **117**, 222409 (2020).

[12] A. Shaib, W. F. Holmes-Hewett, J. Chan, P. P. Murmu, B. J. Ruck, H. J. Trodahl, and F. Natali, SmN and DyN: Effect of the nitrogen to rare earth flux ratio on the structural, transport, and magnetic properties, AIP Adv. **11**, 015125 (2021).

[13] A. Shaib, F. Natali, J. R. Chan, F. Ullstad, W. F. Holmes-Hewett, J. D. Miller, B. J. Ruck, and H. J. Trodahl, Coexisting structural phases in the catalytically driven growth of rock salt GdN, Mater. Res. Express **7**, 046404 (2020).

[14] J. W. Gerlach, J. Mennig, and B. Rauschenbach, Epitaxial gadolinium nitride thin films, Appl. Phys. Lett. **90**, 061919 (2007).

[15] B. M. Ludbrook, I. L. Farrell, M. Kuebel, B. J. Ruck, A. R. H. Preston, H. J. Trodahl, L. Ranno, R. J. Reeves, and S. M. Durbin, Growth and properties of epitaxial GdN, J. Appl. Phys. **106**, 063910 (2009).

[16] A. R. H. Preston, B. J. Ruck, W. R. L. Lambrecht, L. F. J. Piper, J. E. Downes, K. E. Smith, and H. J. Trodahl, Electronic band structure information of GdN extracted from x-ray absorption and emission spectroscopy, Appl. Phys. Lett. **96**, 032101 (2010).

[17] J. H. Richter, B. J. Ruck, M. Simpson, F. Natali, N. O. V. Plank, M. Azeem, H. J. Trodahl, A. R. H. Preston, B. Chen, J. McNulty, K. E. Smith, A. Tadich, B. Cowie, A. Svane, M. van Schilfgaarde, and W. R. L. Lambrecht, Electronic structure of EuN: Growth, spectroscopy, and theory, Phys. Rev. B **84**, 235120 (2011).

[18] B. J. Ruck, H. J. Trodahl, J. H. Richter, J. C. Cezar, F. Wilhelm, A. Rogalev, V. N. Antonov, B. D. Le, and C. Meyer, Magnetic state of EuN: X-ray magnetic circular dichroism at the Eu $M_{4,5}$ and $L_{2,3}$ absorption edges, Phys. Rev. B **83**, 174404 (2011).

[19] J. F. McNulty, K. Temst, M. J. Van Bael, A. Vantomme, and E.-M. Anton, Epitaxial growth of (100)-oriented SmN directly on (100)Si substrates, Phys. Rev. Mater. **5**, 113404 (2021).

[20] F. Natali, N. Plank, J. Galipaud, B. Ruck, H. Trodahl, F. Semond, S. Sorieul, and L. Hirsch, Epitaxial growth of GdN on silicon substrate using an AlN buffer layer, J. Cryst. Growth **312**, 3583 (2010).

[21] F. Natali, S. Vézian, S. Granville, B. Damilano, H. Trodahl, E.-M. Anton, H. Warring, F. Semond, Y. Cordier, S. Chong, and B. Ruck, Molecular beam epitaxy of ferromagnetic epitaxial GdN thin films, J. Cryst. Growth **404**, 146 (2014).

[22] F. Natali, B. Ludbrook, J. Galipaud, N. Plank, S. Granville, A. Preston, B. L. Do, J. Richter, I. Farrell, R. Reeves *et al.*, Epitaxial growth and properties of GdN, EuN and SmN thin films, Phys. Status Solidi C **9**, 605 (2012).

[23] H. Yoshitomi, S. Kitayama, T. Kita, O. Wada, M. Fujisawa, H. Ohta, and T. Sakurai, Optical and magnetic properties in epitaxial GdN thin films, Phys. Rev. B **83**, 155202 (2011).

[24] R. Vidyasagar, S. Kitayama, H. Yoshitomi, T. Kita, T. Sakurai, and H. Ohta, Study on spin-splitting phenomena in the band structure of GdN, Appl. Phys. Lett. **100**, 232410 (2012).

[25] F. Leuenberger, A. Parge, W. Felsch, K. Fauth, and M. Hessler, GdN thin films: Bulk and local electronic and magnetic properties, Phys. Rev. B **72**, 014427 (2005).

[26] N. O. V. Plank, F. Natali, J. Galipaud, J. H. Richter, M. Simpson, H. J. Trodahl, and B. J. Ruck, Enhanced Curie temperature in N-deficient GdN, Appl. Phys. Lett. **98**, 112503 (2011).

[27] F. Natali, B. J. Ruck, H. J. Trodahl, D. L. Binh, S. Vezian, B. Damilano, Y. Cordier, F. Semond, and C. Meyer, Role of magnetic polarons in ferromagnetic GdN, Phys. Rev. B **87**, 035202 (2013).

[28] E.-M. Anton, W. F. Holmes-Hewett, J. F. McNulty, F. Natali, F. Bramley, Y. Choi, D. Haskel, B. J. Ruck, and H. J. Trodahl, GdN/SmN superlattices; influence of a Zeeman/exchange conflict, AIP Adv. **11**, 015348 (2021).

[29] E.-M. Anton, B. J. Ruck, C. Meyer, F. Natali, H. Warring, F. Wilhelm, A. Rogalev, V. N. Antonov, and H. J. Trodahl, Spin/orbit moment imbalance in the near-zero moment ferromagnetic semiconductor SmN, Phys. Rev. B **87**, 134414 (2013).

[30] E.-M. Anton, S. Granville, A. Engel, S. V. Chong, M. Governale, U. Zülicke, A. G. Moghaddam, H. J. Trodahl, F. Natali, S. Vézian, and B. J. Ruck, Superconductivity in the ferromagnetic semiconductor samarium nitride, Phys. Rev. B **94**, 024106 (2016).

[31] W. F. Holmes-Hewett, F. H. Ullstad, B. J. Ruck, F. Natali, and H. J. Trodahl, Anomalous Hall effect in SmN: Influence of orbital magnetism and $4f$-band conduction, Phys. Rev. B **98**, 235201 (2018).

[32] W. F. Holmes-Hewett, R. G. Buckley, B. J. Ruck, F. Natali, and H. J. Trodahl, Optical spectroscopy of SmN: Locating the $4f$ conduction band, Phys. Rev. B **99**, 205131 (2019).

[33] P. Larson, W. R. L. Lambrecht, A. Chantis, and M. van Schilfgaarde, Electronic structure of rare-earth nitrides using the LSDA+U approach: Importance of allowing $4f$ orbitals to break the cubic crystal symmetry, Phys. Rev. B **75**, 045114 (2007).

[34] A. Galler and L. V. Pourovskii, Electronic structure of rare-earth mononitrides: Quasiatomic excitations and semiconducting bands, New J. Phys. **24**, 043039 (2022).

[35] H. R. Child, M. K. Wilkinson, J. W. Cable, W. C. Koehler, and E. O. Wollan, Neutron diffraction investigation of the magnetic properties of compounds of rare-earth metals with group V anions, Phys. Rev. **131**, 922 (1963).

[36] P. Junod, A. Menth, and O. Vogt, Revue des propriétés magnétiques et électroniques des composés des terres rares avec les anions du 5ième groupe du système périodique, Phys. Kondens. Mater. **8**, 323 (1969).

[37] O. Vogt and K. Mattenberger, The magnetism of localized or nearly localized $4f$ and $5f$ shells, J. Alloys Compd. **223**, 226 (1995).

[38] T. A. Yamamoto, T. Nakagawa, K. Sako, T. Arakawa, and H. Nitani, Magnetocaloric effect of rare earth mono-nitrides, TbN and HoN, J. Alloys Compd. **376**, 17 (2004).

[39] P. Wachter, Physical properties of some stoichiometric rare earth nitride single crystals, Adv. Mater. Phys. Chem. **05**, 96 (2015).

[40] W. F. Holmes-Hewett, R. G. Buckley, B. J. Ruck, F. Natali, and H. J. Trodahl, $4f$ conduction in the magnetic semiconductor NdN, Phys. Rev. B **100**, 195119 (2019).

[41] J. Schille, P. Sainctavit, C. Cartier, D. Lefebvre, C. Brouder, J. Kappler, and G. Krill, Magnetic circular X-ray dichroism at high magnetic field and low temperature in ferrimagnetic $HoCo_2$ and paramagnetic Ho_2O_3, Solid State Commun. **85**, 787 (1993).

[42] B. T. Thole, G. van der Laan, J. C. Fuggle, G. A. Sawatzky, R. C. Karnatak, and J.-M. Esteva, $3d$ x-ray-absorption lines and the $3d^9 4f^{n+1}$ multiplets of the lanthanides, Phys. Rev. B **32**, 5107 (1985).

[43] J. Yeh and I. Lindau, Atomic subshell photoionization cross sections and asymmetry parameters: $1 \leqslant Z \leqslant 103$, At. Data Nucl. Data Tables **32**, 1 (1985).